PHYSICAL REVIEW B **89**, 155103 (2014)

Wigner crystal of a two-dimensional electron gas with a strong spin-orbit interaction

P. G. Silvestrov[1,2] and O. Entin-Wohlman[3,4]
[1]*Physics Department and Dahlem Center for Complex Quantum Systems, Freie Universität Berlin, 14195 Berlin, Germany*
[2]*Institute for Mathematical Physics, TU Braunschweig, 38106 Braunschweig, Germany*
[3]*Physics Department, Ben Gurion University, Beer Sheva 84105, Israel*
[4]*Raymond and Beverly Sackler School of Physics and Astronomy, Tel Aviv University, Tel Aviv 69978, Israel*
(Received 14 September 2013; revised manuscript received 19 March 2014; published 2 April 2014)

The Wigner-crystal phase of two-dimensional electrons interacting via the Coulomb repulsion and subject to a strong Rashba spin-orbit coupling is investigated. For low enough electronic densities the spin-orbit band splitting can be larger than the zero-point energy of the lattice vibrations. Then the degeneracy of the lower subband results in a spontaneous symmetry breaking of the vibrational ground state. The 60° rotational symmetry of the triangular (spin-orbit coupling free) structure is lost, and the unit cell of the new lattice contains two electrons. Breaking the rotational symmetry also leads to a (slight) squeezing of the underlying triangular lattice.

DOI: 10.1103/PhysRevB.89.155103 PACS number(s): 73.20.Qt, 75.70.Tj

I. INTRODUCTION

The Wigner crystal [1], the insulating companion of a two-dimensional metal, is predicted to appear in an electron gas of ultralow densities formed in semiconductor heterostructures when the Coulomb repulsion-induced ordering wins over the zero-point quantum fluctuations [2,3]. Low densities amount to very clean samples. That is why experimentally Wigner crystals were observed either in naturally clean systems, like electrons on the surface of liquid helium [4], or in two-dimensional semiconductors when the kinetic energy is suppressed by a strong magnetic field [5], or due to a large mass of the charge carriers [6]. However, lowering the electronic density not only enhances the electronic correlations, but also tends to increase the relative importance of the spin-orbit interaction, generically present in low-dimensional systems [7]. Thus, attempting to increase the role of electronic repulsion may lead one into a regime in which quantum fluctuations around the classical equilibrium sites of the Wigner crystal are dominated by the spin-orbit interaction. Such crystals, as we show, demonstrate a number of unexpected properties, having no analog hitherto.

The structure of a crystal is usually determined by the interaction between particles that oscillate slightly around their static equilibrium positions. For electrons subject to the Rashba spin-orbit interaction [8], which we consider in this paper, this picture is modified, since in this case even the notion "static particle position" requires a clarification. The spin-orbit interaction splits the spectrum of free electrons, leading to a sombrero-shaped lower subband with a circle of degenerate minima. Naively, one would have expected that in the crystalline phase the electrons' wave functions will be spread in momentum space over the entire circle of those minima. However, for the electrons' vibrations in the crystal, different minima of the single-particle spectrum are not equivalent. Since the uncertainty principle couples the coordinates and the momenta, broken spatial symmetries in the crystalline phase are transferred into a broken rotational symmetry in momentum space. As we show in this paper, the true ground state corresponds to a crystalline configuration with each electron picking up (i.e., vibrating around) a particular point at the bottom of the sombrero. This type of configuration allows for effectively reducing the energy of Coulomb repulsion among the electrons, without increasing too much the kinetic energy.

We consider strong spin-orbit interactions, such that the effective Hilbert space is reduced to include only electronic states of momenta close to the ring of minima in the lower subband [see Fig. 1(a)]. Each electron in the crystal picks up only one of those minima. However, since the electron's displacement in momentum space along the line of minima costs no kinetic energy, one may effectively freeze its spatial vibrations in this direction. Freezing the spatial vibrational mode reduces the average potential energy, since now the electron never leaves its classical equilibrium location in this direction. The vibrations along the direction perpendicular to the ring of minima have the same effective mass as in the absence of the spin-orbit interaction. Hence the electrons' fluctuations when the spin-orbit coupling is strong enough are equivalent to vibrations of particles having anisotropic masses. Here though, the light and the (infinitely) heavy masses' directions are chosen for each electron individually.

As different minima of the Rashba Hamiltonian are classically equivalent, the proper choice of the electrons' configuration should be the one minimizing the zero-point fluctuation energy of the crystal. Finding the minimum of the zero-point energy for general directions of the oscillations is a difficult task which will not be fully accomplished in this paper. Instead, we adopt a step-by-step approach, considering a series of configurations depending on 1, 2, 3, . . ., angles with respect to which the energy functional is minimized. The first three steps in this scheme are illustrated in Figs. 1(b)–1(d). The dark ellipses there indicate the directions along which the electrons vibrate. First, one requires all electrons to vibrate in unison, and minimizes the energy with respect to a single angle. Figure 1(b) shows the best configuration of such a one-parameter family. At the next step one allows two neighboring electrons on the triangular lattice to vibrate along independent directions and then repeats this configuration periodically. The unit cell now contains two electrons. Figure 1(c) shows the configuration realizing the minimum of the vibrational energy for such a two-parameter family of crystals. One may consider similarly a lattice with more independent vibrational directions; see Fig. 1(d). Among all crystal configurations which we have

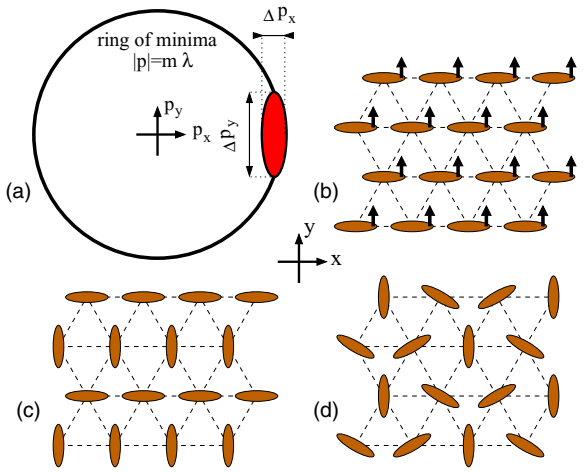

FIG. 1. (Color online) Schematic visualization of the electronic density in a two-dimensional electron crystal. (a) The ring of minima in momentum space for the lower Rashba subband $E_{p-} = (p - m\lambda)^2/(2m)$ (λ is the strength of the Rashba interaction). The colored ellipse shows the electronic density [for structure (b)]. The density is centered around a particular minimum, but is strongly elongated along the line of minima, $\Delta p_x \ll \Delta p_y \ll m\lambda$, which helps to lower the interaction energy. (b)–(d) Three possible periodic configurations (see text). The dark ellipses indicate the directions of electrons' oscillations. Structure (c) has the lowest zero-point energy of the lattice vibrations. The arrows in (b) indicate the in-plane spin orientations.

analyzed, the one in Fig. 1(c) has the smallest vibrational energy. Different crystal configurations have also a very different vibrational spectra (Fig. 2 below), a fact which can be exploited to distinguish them experimentally.

Recently, Berg *et al.* [9] have shown that the Rashba spin-orbit interaction can stabilize the two-dimensional Wigner crystal even when the electron-electron interaction potential

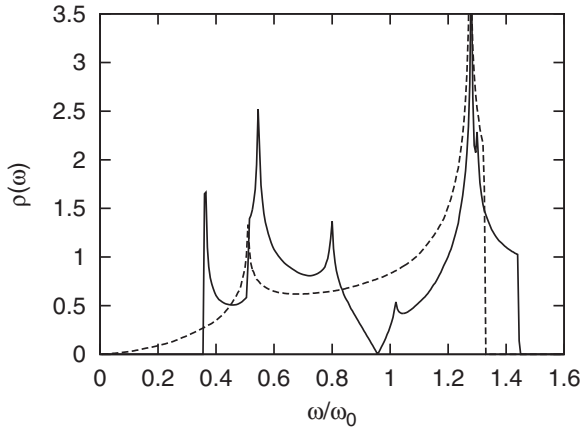

FIG. 2. The vibration density of states as a function of the frequency (scaled by ω_0) for the Wigner-crystal configuration of Fig. 1(b) (dashed line) and of Fig. 1(c) (solid line). Though the spectrum extends all the way down to $\omega = 0$ for 1(b) the average frequency turns out to be smaller for 1(c). Note the linear vanishing of the density (characteristic of a Dirac cone) in the middle of spectrum for 1(c) and especially the inverse square-root divergence of the density at the lower edge, $\omega \approx 0.36\omega_0$.

is short-range, $V \sim 1/r^\alpha$ with $\alpha > 2$. In the absence of the spin-orbit coupling, such a crystal would have been unstable for any small electronic density. The price for the short-range interaction considered in Ref. [9] is a strong asymmetry (squeezing) of the crystal. In our paper we analyze the crystal created by electrons interacting via the *unscreened* Coulomb repulsion, $V = e^2/r$. Then the triangular lattice of the crystal [10] remains stable on the classical level. However, breaking the symmetry in momentum plane changes drastically the fluctuation properties and the electronic density distribution.

We stress that our considerations are confined to low electronic densities, where the dominance of the Coulomb repulsion over the fluctuation energy ensures the stability of the crystal. The transition from the crystalline phase to the Fermi-liquid one is not touched upon.

The paper is organized as follows. In Sec. II we discuss the Hamiltonian and in particular elaborate on the various parameters governing the spectrum. In Sec. III we introduce the effective Hamiltonian for the phonon modes which is responsible for the largest part of the vibrational energy, and use it to derive analytically the excitation spectrum of the simplest configuration of the crystal. More complicated configurations of the crystal are investigated in the Appendix. In Sec. IV we consider the minimization of the crystal vibration zero-point energy and discuss certain properties of the ground state we find. Section V is devoted to an estimate of the squeezing of the lattice. Our conclusions, as well as a discussion of a possible experimental detection, are given in Sec. VI.

II. WIGNER CRYSTAL WITH SPIN-ORBIT COUPLING

The Hamiltonian of the system under consideration is

$$\mathcal{H} = \sum_i \mathcal{H}_{0i} + \sum_{i<j} e^2/|\mathbf{R}_{ij} + \mathbf{r}_{ij}|\,, \tag{1}$$

with $\mathbf{R}_{ij} \equiv \mathbf{R}_i - \mathbf{R}_j$. At equilibrium, the electrons are located at sites $\mathbf{R}_i$ on a triangular lattice [10] of spacing a. The oscillations around those sites are described by expanding the interaction in the small displacements $|\mathbf{r}_i| \ll a$ up to second order [11]. This expansion yields a single-electron harmonic potential and an electron-electron interaction (bi)linear in the displacement [see Eq. (7) below]. The former allows us to introduce the frequency [12]

$$\omega_0 = \sqrt{\gamma e^2/(ma^3)}\,, \tag{2}$$

with $\gamma = \sum_{i\neq 0} a^3/(2R_i^3) = 5.5171$ and m being the effective mass. The single-electron part of the Hamiltonian (1) reads

$$\mathcal{H}_0 = \mathbf{p}^2/(2m) + \lambda(\sigma_x p_y - \sigma_y p_x) + m\lambda^2/2\,, \tag{3}$$

where λ denotes the Rashba spin-orbit coupling strength and $\sigma_{x,y}$ are the Pauli matrices. The spectrum of $\mathcal{H}_0$ consists of two subbands, $E_{p\pm} = (p \pm m\lambda)^2/(2m)$, which correspond to electrons with in-plane spins directed normal to the momentum, and pointing to its left or right, respectively. We focus on the regime where the spin-orbit energy exceeds the one due to the zero-point motion of the electrons around their

equilibrium sites,

$$m\lambda^2 \gg \hbar\omega_0 \sim \sqrt{e^2\hbar^2/(ma^3)}\,, \tag{4}$$

which means that the electrons are always confined to the lowest subband. The relative strength of the Coulomb interaction compared to the kinetic energy is characterized by the dimensionless parameter r_s, related to the electronic density n and the Bohr radius $a_B = \hbar^2/(me^2)$ as $\pi r_s^2 = 1/(na_B^2)$ [13]. Obviously, in the case of a strong Rashba spin-orbit interaction the large value of the same parameter ensures the existence of the Wigner crystal: $r_s \gg 1$ here means that the gain in the Coulomb energy per electron in the ordered phase exceeds the energy rise due to the zero-point fluctuations of electrons in the lattice, $e^2/a \gg \hbar\omega_0$. (Quantum Monte Carlo simulations [2,3] indicate that in the absence of spin-orbit coupling the Wigner crystal exists at $r_s > 35$.)

Once the electrons reside in the lower Rashba subband, their (ground-state) momenta lie within a narrow ring in momentum plane of radius $m\lambda$ and width Δp, determined by the zero-point energy

$$(p - m\lambda)^2 \lesssim \Delta p^2 \sim \sqrt{e^2\hbar^2 m/a^3} \ll (m\lambda)^2\,. \tag{5}$$

However, in the crystal different parts of this ring are not equivalent and each electron may choose its own small sector. Imagine a much-elongated wave packet built from the lower Rashba subband solutions, such that

$$|p_x - m\lambda| \lesssim \Delta p_x, \quad |p_y| \lesssim \Delta p_y, \quad \Delta p_x \ll \Delta p_y \ll m\lambda, \tag{6}$$

as in Fig. 1(a). The two spatial dimensions of this wave packet are very different, $\Delta x \gg \Delta y$, and hence the minute displacement along the y direction gives a negligible correction to the interaction energy. The expectation value of $\mathcal{H}_0$, which has an eigenvalue $E_- = 0$ at $|p| = m\lambda$, is determined by the smaller momentum extension of the packet, $\langle\mathcal{H}_0\rangle \sim \Delta p_x^2/(2m)$. This implies that the system may choose an anisotropic pattern where around each lattice site the density forms a narrow ellipse of length $\Delta x \sim [a^3\hbar^2/(me^2)]^{1/4}$. The orientations of these ellipses will be determined by the zero-point energy of the vibrations pertaining to a specific pattern.

III. VIBRATION SPECTRUM

We begin with the configuration shown in Fig. 1(b). In this structure the electrons oscillate along x, and (since the Hilbert space is reduced to that of the lower Rashba subband) are strongly spin-polarized along y, $\langle\sigma_y\rangle \simeq 1$. To find the excitation spectrum around this particular structure, we shift the x component of the momentum, $p_x \to m\lambda + p_x$, multiplying the many-electron wave function by $\exp[(i/\hbar)\sum_i m\lambda x_i]$. The reduced Hamiltonian contains only the term quadratic in p_x, while p_y appears at higher orders in $p_y/(m\lambda)$ and may be discarded. The uncertainty principle then imposes no restrictions on the displacements along the y direction, allowing us to choose $y_i \equiv 0$. This results in a single-coordinate effective Hamiltonian,

$$\mathcal{H}_{\rm eff} = \sum_i \left[p_{x_i}^2/(2m) + m\omega_0^2 x_i^2/2\right] + e^2\sum_{i<j} x_i x_j u_{ij}, \tag{7}$$

where $u_{ij} = 1/R_{ij}^3 - 3X_{ij}^2/R_{ij}^5$, X_{ij} is the x component of $\mathbf{R}_{ij}$, and ω_0 is defined in Eq. (2). The Hamiltonian Eq. (7) contains half of the degrees of freedom of the original one, since it allows for a single vibrational direction per electron. In the regime given by Eq. (4), the missing degrees of freedom pertain to low-energy nonphononic excitations, whose analysis is beyond the scope of this paper.

Exploiting the Bogoliubov transformation

$$c_{\mathbf{k}} \equiv \sum_i e^{-i\mathbf{k}\cdot\mathbf{R}_i}\frac{m\omega_0 x_i + ip_{x_i}}{\sqrt{2Nm\omega_0\hbar}} = \cosh u_{\mathbf{k}} d_{\mathbf{k}} + \sinh u_{\mathbf{k}} d_{-\mathbf{k}}^\dagger, \tag{8}$$

where N is the number of lattice sites, transforms the Hamiltonian into

$$\mathcal{H}_{\rm eff} = \sum_{\mathbf{k}} \hbar\omega_{\mathbf{k}}\left(d_{\mathbf{k}}^\dagger d_{\mathbf{k}} + \frac{1}{2}\right), \quad \omega_{\mathbf{k}} = \omega_0\sqrt{1 + 2v(\mathbf{k})}\,. \tag{9}$$

Here, $\tanh 2u_{\mathbf{k}} = -v(\mathbf{k})/[1 + v(\mathbf{k})]$ and $v(\mathbf{k}) = \sum_{i\neq 0} e^{i\mathbf{k}\cdot\mathbf{R}_{0i}}$ $[a^3/(2\gamma R_{0i}^3)](1 - 3X_{0i}^2/R_{0i}^2)$. In particular, at small wave vectors the dispersion law becomes

$$\omega_{\mathbf{k}} = [4\pi e^2/(\sqrt{3}ma^2)]^{1/2}|k_x|/\sqrt{k}. \tag{10}$$

The $\sqrt{k}$ dependence at the low frequencies is well-known for the plasmon spectrum of a two-dimensional electron gas. The striking feature though is the *angular dependence* of the dispersion law (10), with vanishing frequency along the y direction. It signals a spontaneous symmetry-breaking caused by the degeneracy at the bottom of the lower Rashba subband.

The vibration spectra for the structures with several electrons per unit cell, as in Figs. 1(c) and 1(d), are found similarly. Details of this calculations are given in the Appendix.

IV. MINIMIZING THE ZERO-POINT ENERGY

We have investigated numerically all possible configurations of the Wigner crystal with vibrational directions depending on 1, 2, and 3 angles, as described in Sec. I. Important examples representing these families of configurations are shown in Figs. 1(b)–1(d). The ground-state energy is determined by the frequency $\omega_{\mathbf{k}}$ averaged over the Brillouin zone, which in the case of Fig. 1 gives

$$\frac{\langle\omega_{\mathbf{k}}^b\rangle}{\omega_0} = 0.951, \quad \frac{\langle\omega_{\mathbf{k}}^c\rangle}{\omega_0} = 0.939, \quad \frac{\langle\omega_{\mathbf{k}}^d\rangle}{\omega_0} = 0.971\,. \tag{11}$$

Quite unexpectedly, among the examined configurations the one with two electrons per unit cell shown in Fig. 1(c) has the smallest zero-point energy. Configuration 1(b) has the smallest $\langle\omega_{\mathbf{k}}\rangle$ for the families with one and three electrons per unit cell, but is not the global minimum of the vibrational energy. The highly symmetric configuration 1(d) has the largest zero-point energy in the family with three independent vibrational directions.

We remind the reader that the disparity in the average frequencies given in Eq. (11) is a measure for the energy gain ($\sim\hbar\omega_0$ per electron) of a system being in a state with a broken symmetry in momentum space. Had one tried to spread the electron wave packet over the entire ring of

minima [Fig. 1(a)], one would have found that this gain in the vibrational energy is lost.

All phonon frequencies coincide independent of the direction of vibration, $\omega_{\mathbf{k}} \equiv \omega_0$, upon exploiting the Einstein approximation, in which each electron is confined to a harmonic potential created when the locations of all other electrons are frozen [11]. In all the crystalline configurations we have considered the average frequency was always close to the Einstein approximation, as in Eq. (11).

One way to probe experimentally the structure of a crystal is to measure the vibration spectrum. Figure 2 shows the density of states (DOS) as a function of the frequency for the structures in Figs. 1(b) and 1(c). Several interesting features can be observed there (but unfortunately, none explains which structure is energetically favorable, and why the resulting $\langle\omega_{\mathbf{k}}\rangle$'s are so close to each other). For the configuration 1(b) the DOS is finite all the way down to zero frequency due to the plasmon mode Eq. (10). The spectrum has a step singularity at the high-frequency end, and two logarithmic van Hove singularities. Though the modes describing global translations for the full Hamiltonian Eq. (1) always have zero energy, it is only for the structure 1(b) that one of these modes is reproduced by the effective Hamiltonian Eq. (7).

The vibration spectrum of the crystalline phase shown in Fig. 1(c) is gapped (the solid line in Fig. 2). The DOS has several step singularities and logarithmic divergences. The linear vanishing of the DOS at $\omega \approx \omega_0$ corresponds to a conical crossing of the two bands (a Dirac point). Surprisingly enough, we observe an almost perfectly inverted square-root singularity at low frequencies, $\rho(\omega) \sim [\omega - 0.36\omega_0]^{-1/2}$; such a divergence usually characterizes *one-dimensional* systems. Careful numerical investigation shows that the dispersion law around these frequencies has the form

$$\left[\omega^c_{\mathbf{k}}/\omega_0\right]\big|_{k_x\approx 0} \approx 0.3584 + 0.564\times 10^{-3}\cos(\sqrt{3}ak_y) + f(k_y)(ak_x)^2, \tag{12}$$

with $f(k_y) \sim 1$. These modes correspond to a horizontal displacement of every second row in the configuration of 1(c). The small coefficient of the second term in Eq. (12) implies that different electron rows "see" each other as a continuous charge lines. This is surprising, since the distance between the rows is only $\sqrt{3}$ times larger than the interval between electrons within each row.

The zero-point fluctuations considered in this section represent the most important, but obviously not the only, quantum corrections to the energy of the Wigner crystal. Since the relative variation of the zero-point energy among the different configurations happens to be less than 3.5% [this is the difference between Figs. 1(c) and 1(d)], one may wonder whether effects not taken into account in our approach may be important for finding the proper ground state. We can envisage two such effects leading to corrections to our results. First, there is a correction to the zero-point energy caused by the phonon interaction, arising from the higher-order terms in the expansion of the Coulomb interaction ($\sim r^3, r^4, \dots$). Another unaccounted for (parametrically small) contribution to the energy comes from the low-energy nonphononic modes, which are not included in the effective Hamiltonian Eq. (7). Investigation of these corrections goes far beyond the scope of this paper. However, if the contribution of nonphononic modes and phonons' interaction, depending on the specific choice of single electrons' minima in the momentum space, turns out to be large enough, it indeed can change the ground state in some intermediate range of values of the electron density. (This would make the phase diagram of the Wigner crystal with spin-orbit interaction even richer and more interesting.) All that can be stated at this stage is that, in the limit of very small electronic densities, both effects mentioned above are parametrically small and may be neglected. The small parameter, leading to the suppression of the phonons' interaction is $a_B/a \ll 1$. The smallness of nonphononic modes' contribution to the energy is governed by the small value of $\Delta p/(m\lambda) \ll 1$ with $\Delta p \propto a^{-3/4}$; see Eq. (5) [or equivalently $\hbar\omega_0/(m\lambda^2) \ll 1$ with $\omega_0 \propto a^{-3/2}$].

V. SQUEEZING THE CRYSTAL

The crystal structures of Figs. 1(b) and 1(c) have a preferential axis, violating the 60° symmetry of the triangular lattice. This opens the possibility for a (slight) squeezing of the lattice, caused by an interplay of the classical Coulomb repulsion and the quantum vibrations (cf. the strong squeezing in the case of a short-range interaction [9]).

The "density preserving" squeezing is defined as $\mathbf{R}_i \to \tilde{\mathbf{R}}_i = [(1+\alpha)X_i, Y_i/(1+\alpha)]$, where α is a small but *finite* parameter. We may also write the energy per electron in a crystal as a power series in Plank's constant, $E(\alpha) = \epsilon_0(\alpha) + \hbar\epsilon_1(\alpha) + \cdots$. The first term is the electron's electrostatic energy,

$$\epsilon_0(\alpha) = (e^2/a)(c_0 + \alpha c_1 + \alpha^2 c_2 + \cdots), \tag{13}$$

and the second comes from the average zero-point energy,

$$\epsilon_1(\alpha) = \omega_0(d_0 - \alpha d_1 + \cdots), \tag{14}$$

where c_i and d_i are numerical coefficients. The coefficients c_0 and d_0 [the latter is found in Eq. (11)] are of no interest. Since the triangular lattice is the minimum of the electronic Coulomb energy [10], one has $c_1 \equiv 0$ and $c_2 > 0$. The linear in α term in the quantum correction to the energy, d_1, would also vanish due to the crystal symmetry in the absence of the spin-orbit coupling, or, e.g., for the 120° rotational symmetric configuration Fig. 1(d), but is allowed for the configurations Figs. 1(b) and 1(c). Numerically we have found $c_2 \approx 0.527$, $d_1^b \approx 0.245$ and $d_1^c \approx 0.425$. Minimizing the energy $E(\alpha)$ results in

$$\alpha_c = \frac{\hbar\omega_0}{2e^2/a}\frac{d_1}{c_2} = \sqrt{\frac{\gamma a_{\mathrm{B}}}{4a}}\frac{d_1}{c_2} \sim \sqrt{\frac{a_B}{a}}. \tag{15}$$

The value of the squeezing parameter, α_c, grows with the density as $a^{-1/2} \sim n^{1/4}$. This increase is limited, however, by the inequality (4).

VI. SUMMARY

As we have shown, the ability of the electrons to occupy different minima in momentum space leads to a complicated ground-state of the Wigner crystal. We have found the ground state by considering an effective Hamiltonian, which accounts for a *single energetic* vibrational mode per electron, leaving

untouched a number of nonphononic excitations from the low-energy sector of the full problem. These soft modes would correspond to a small displacement of the electron wave packet in momentum space along the circle of degenerate minima [see Fig. 1(a)], or to spin flips associated with the 180° jumps of the electron to the opposite side of the circle of minima (see Refs. [12,14] for a discussion of the spin structure of a Wigner crystal.)

Although we expect the true ground state of the crystal to be the structure in Fig. 1(c), other configurations may exist as metastable states. If the configuration 1(b) would be realized experimentally, one will be able to probe the angular-dependent plasmon modes, Eq. (10).

Finally, the existence of the spin-orbit dominated phase of the Wigner crystal described in this paper requires the validity of the inequality (4). This inequality may be rewritten as $m^*\lambda^2 \gg \mathrm{Ry}/r_s^{3/2}$, where $\mathrm{Ry} = m^*e^4/2\hbar^2\epsilon^2$ and m^* and ϵ are the effective mass and dielectric constant, respectively. For [15] InAs, $m^*\lambda^2 \approx 0.2$ meV and $\mathrm{Ry} \approx 2.5$ eV. Assuming that in the presence of spin-orbit interactions the crystal stability still requires the large value of $r_s \sim 35$, we expect our results to be always applicable for Wigner crystals in such materials.

ACKNOWLEDGMENTS

We thank Y. Imry, P. W. Brouwer, E. Bergholtz and M. Schneider for helpful discussions. The hospitality of the Institute for Advanced Studies at the Hebrew University and the Albert Einstein Minerva Center for Theoretical Physics at the Weizmann Institute are gratefully acknowledged. This work was supported by the Alexander von Humboldt Foundation, DFG Grant No. RE 2978/1-1, the Israeli Science Foundation (ISF), and the US-Israel Binational Science Foundation (BSF).

APPENDIX: VIBRATION SPECTRUM FOR SEVERAL ELECTRONS PER UNIT CELL

We first show how to obtain the phonon spectrum belonging to configuration in Fig. 1(c). This is an example of a lattice with two electrons per unit cell (which turns out to be our best candidate for the ground state). We then sketch briefly the derivation of the spectrum in the case of three electrons per unit cell, vibrating along three arbitrary directions.

1. The configuration of Fig. 1(c)

When there are two electrons within each unit cell, it is convenient to introduce two sublattices, a and b. The effective vibration Hamiltonian for the configuration of Fig. 1(c) is then

$$\begin{aligned}\mathcal{H}_{\mathrm{eff}} = &\sum_{i\in a}\left(\frac{p_{x_i}^2}{2m}+\frac{m\omega_0^2x_i^2}{2}\right)+e^2\sum_{i<j\in a}\frac{x_ix_j}{R_{ij}^3}\left(1-3\frac{X_{ij}^2}{R_{ij}^2}\right)\\ &+\sum_{i\in b}\left(\frac{p_{y_i}^2}{2m}+\frac{m\omega_0^2y_i^2}{2}\right)+e^2\sum_{i<j\in b}\frac{y_iy_j}{R_{ij}^3}\left(1-3\frac{Y_{ij}^2}{R_{ij}^2}\right)\\ &-3e^2\sum_{i\in a,j\in b}x_iy_j\frac{X_{ij}Y_{ij}}{R_{ij}^5}\,. \end{aligned}\tag{A1}$$

Introduction of the creation/annihilation operators

$$a=\sqrt{\frac{m\omega_0}{2\hbar}}\left(x+\frac{ip_x}{m\omega_0}\right),\quad b=\sqrt{\frac{m\omega_0}{2\hbar}}\left(y+\frac{ip_y}{m\omega_0}\right)\tag{A2}$$

leads to the Hamiltonian

$$\begin{aligned}\mathcal{H}_{\mathrm{eff}} = \hbar\omega_0\Bigg(&\sum_{i\in a}\left(a_i^\dagger a_i+\frac{1}{2}\right)+\sum_{i<j\in a}v_{ij}^x(a_i+a_i^\dagger)(a_j+a_j^\dagger)\\ &+\sum_{i\in b}\left(b_i^\dagger b_i+\frac{1}{2}\right)+\sum_{i<j\in b}v_{ij}^y(b_i+b_i^\dagger)(b_j+b_j^\dagger)\\ &+\sum_{i\in a,j\in b}w_{ij}(a_i+a_i^\dagger)(b_j+b_j^\dagger)\Bigg),\end{aligned}\tag{A3}$$

where

$$\begin{aligned}v_{ij}^x&=\frac{a^3\left(R_{ij}^2-3X_{ij}^2\right)}{2\gamma R_{ij}^5},\quad v_{ij}^y=\frac{a^3\left(R_{ij}^2-3Y_{ij}^2\right)}{2\gamma R_{ij}^5}\\ w_{ij}&=-3\frac{a^3X_{ij}Y_{ij}}{2\gamma R_{ij}^5}.\end{aligned}\tag{A4}$$

In Fourier space, this Hamiltonian takes the form

$$\begin{aligned}\mathcal{H}_{\mathrm{eff}} = \hbar\omega_0\sum_{\mathbf{k}}\Bigg[&\left(a_{\mathbf{k}}^\dagger a_{\mathbf{k}}+\frac{1}{2}\right)+\frac{v^x(\mathbf{k})}{2}(a_{\mathbf{k}}+a_{-\mathbf{k}}^\dagger)(a_{-\mathbf{k}}+a_{\mathbf{k}}^\dagger)\\ &+\left(b_{\mathbf{k}}^\dagger b_{\mathbf{k}}+\frac{1}{2}\right)+\frac{v^y(\mathbf{k})}{2}(b_{\mathbf{k}}+b_{-\mathbf{k}}^\dagger)(b_{-\mathbf{k}}+b_{\mathbf{k}}^\dagger)\\ &+w(\mathbf{k})(a_{\mathbf{k}}+a_{-\mathbf{k}}^\dagger)(b_{-\mathbf{k}}+b_{\mathbf{k}}^\dagger)\Bigg],\end{aligned}\tag{A5}$$

with

$$\begin{aligned}v^x(\mathbf{k})&=\sum_{0\in a,i\neq 0\in a}v_{0i}^xe^{i\mathbf{k}\cdot\mathbf{R}_i},\\ v^y(\mathbf{k})&=\sum_{0\in a,i\neq 0\in a}v_{0i}^ye^{i\mathbf{k}\cdot\mathbf{R}_i},\\ w(\mathbf{k})&=\sum_{0\in a,i\in b}w_{0i}e^{i\mathbf{k}\cdot\mathbf{R}_i}.\end{aligned}\tag{A6}$$

Also $v^x(\mathbf{k})=v^x(-\mathbf{k})$, $v^y(\mathbf{k})=v^y(-\mathbf{k})$, and $w(\mathbf{k})=w(-\mathbf{k})$. An important point to note here is that $v^y(\mathbf{k})\neq v^x(\mathbf{k})$. In the next step one decouples the two vibration polarizations,

$$\begin{aligned}c_{\mathbf{k}}&=\cos(\tau_{\mathbf{k}})a_{\mathbf{k}}+\sin(\tau_{\mathbf{k}})b_{\mathbf{k}},\\ d_{\mathbf{k}}&=-\sin(\tau_{\mathbf{k}})a_{\mathbf{k}}+\cos(\tau_{\mathbf{k}})b_{\mathbf{k}},\end{aligned}\tag{A7}$$

with $\tan(2\tau_{\mathbf{k}})=2w(\mathbf{k})/[v^x(\mathbf{k})-v^y(\mathbf{k})]$, to obtain

$$\begin{aligned}\mathcal{H}_{\mathrm{eff}} = \hbar\omega_0\sum_{\mathbf{k}}\Bigg[&\left(c_{\mathbf{k}}^\dagger c_{\mathbf{k}}+\frac{1}{2}\right)+\frac{v_1(\mathbf{k})}{2}(c_{\mathbf{k}}+c_{-\mathbf{k}}^\dagger)(c_{-\mathbf{k}}+c_{\mathbf{k}}^\dagger)\\ &+\left(d_{\mathbf{k}}^\dagger d_{\mathbf{k}}+\tfrac{1}{2}\right)+\frac{v_2(\mathbf{k})}{2}(d_{\mathbf{k}}+d_{-\mathbf{k}}^\dagger)(d_{-\mathbf{k}}+d_{\mathbf{k}}^\dagger)\Bigg],\end{aligned}\tag{A8}$$

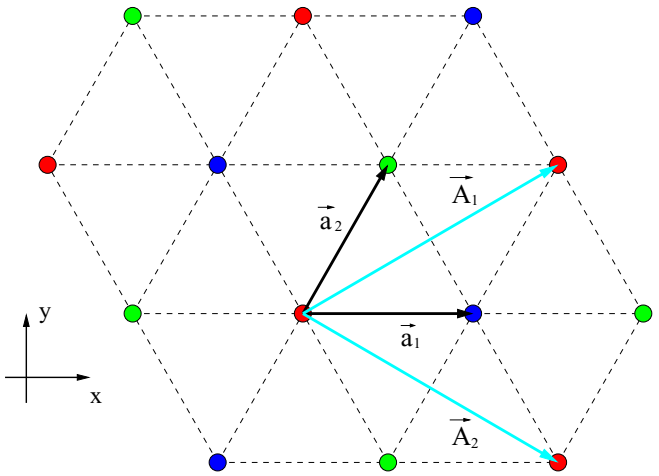

FIG. 3. (Color online) Definition of the basis vectors for the original triangular lattice, $\mathbf{a}_1$ and $\mathbf{a}_2$, and for the superlattice with three electrons per unit cell, $\mathbf{A}_1$ and $\mathbf{A}_2$. Electrons from the three different sublattices are shown by different colors.

where

$$v_{1,2}(\mathbf{k}) = \tfrac{1}{2}[v^x(\mathbf{k}) + v^y(\mathbf{k}) \pm \sqrt{[v^x(\mathbf{k}) - v^y(\mathbf{k})]^2 + 4w^2(\mathbf{k})}]. \tag{A9}$$

Each polarization can be now Bogoliubov transformed exactly as is carried out in the main text.

2. Phonon spectrum for superlattices with three electrons per unit cell

The triangular lattice of a usual Wigner crystal is defined by two lattice vectors, $\mathbf{a}_1 = (a,0)$ and $\mathbf{a}_2 = (a/2, \sqrt{3}a/2)$. The superlattice with three atoms per unit cell is defined by the lattice vectors $\mathbf{A}_1 = (3a/2, \sqrt{3}a/2)$ and $\mathbf{A}_2 = (3a/2, -\sqrt{3}a/2)$, such that $|\mathbf{A}_1| = |\mathbf{A}_2| = \sqrt{3}a$, as is shown in Fig. 3. The electrons on this lattice naturally form three sublattices whose sites coordinates are $i\mathbf{A}_1 + j\mathbf{A}_2$, $(a,0) + i\mathbf{A}_1 + j\mathbf{A}_2$, and $(-a,0) + i\mathbf{A}_1 + j\mathbf{A}_2$. Here i and j are two arbitrary integer numbers.

Let the displacement vectors for the three sublattices be $\mathbf{u}_i$, $\mathbf{v}_i$, and $\mathbf{w}_i$, where $\mathbf{u} = u\mathbf{n}_u$, $\mathbf{v} = v\mathbf{n}_v$, and $\mathbf{w} = w\mathbf{n}_w$, with the three unit vectors $\mathbf{n}_u$, $\mathbf{n}_v$, and $\mathbf{n}_w$ pointing along the directions of the allowed vibrations for each sublattice. For example, for the electronic configuration shown in Fig. 1(d) of the main text one has $\mathbf{n}_u = (0,1)$, $\mathbf{n}_v = (\sqrt{3}/2, -1/2)$, and $\mathbf{n}_w = (-\sqrt{3}/2, -1/2)$. However, our derivation below does not assume any specific orientation of $\mathbf{n}_u$, $\mathbf{n}_v$, and $\mathbf{n}_w$.

The Hamiltonian takes the form

$$H = h_u + h_v + h_w + V_u + V_v + V_w + W_{uv} + W_{uw} + W_{vw}, \tag{A10}$$

where, for example,

$$h_u = \sum_{i\in u} \left(\frac{p_{u_i}^2}{2m} + \frac{m\omega^2 u^2}{2} \right), \tag{A11}$$

and

$$V_u = e^2 \sum_{i<j\in u} u_i u_j \left(\frac{1}{R_{ij}^3} - 3\frac{(\mathbf{n}_u \cdot \mathbf{R}_{ij})^2}{R_{ij}^5} \right),$$
$$W_{uv} = e^2 \sum_{i\in u, j\in v} u_i v_j \left(\frac{1}{R_{ij}^3} - 3\frac{(\mathbf{n}_u \cdot \mathbf{R}_{ij})(\mathbf{n}_v \cdot \mathbf{R}_{ij})}{R_{ij}^5} \right). \tag{A12}$$

Let

$$u_i = \sqrt{\frac{3}{N}} \sum_{\mathbf{k}} e^{i\mathbf{k}\cdot\mathbf{R}_i} u_{\mathbf{k}},$$
$$v_i = \sqrt{\frac{3}{N}} \sum_{\mathbf{k}} e^{i\mathbf{k}\cdot\mathbf{R}_i} v_{\mathbf{k}}, \tag{A13}$$
$$w_i = \sqrt{\frac{3}{N}} \sum_{\mathbf{k}} e^{i\mathbf{k}\cdot\mathbf{R}_i} w_{\mathbf{k}},$$

where N is the total number of electrons and $\mathbf{R}_j$ is the true coordinate of the corresponding N-electron lattice site. Similarly we introduce the Fourier transformed momenta $p_{u_\mathbf{k}}, p_{v_\mathbf{k}}, p_{w_\mathbf{k}}$, so that $[p_\mathbf{k}, x_\mathbf{q}] = -i\delta_{\mathbf{k}+\mathbf{q}}$. It follows that

$$h_{u_\mathbf{k}} = \sum_{\mathbf{k}} \left(\frac{p_{u_{-\mathbf{k}}} p_{u_\mathbf{k}}}{2m} + \frac{m\omega^2 u_{-\mathbf{k}} u_\mathbf{k}}{2} \right), \tag{A14}$$

$$V_u \to V_u^{(\mathbf{k})} = \frac{e^2}{2} \sum_{\mathbf{k}} u_{-\mathbf{k}} u_\mathbf{k} \mathcal{V}_u(\mathbf{k}),$$
$$\mathcal{V}_u(\mathbf{k}) = \sum_j e^{i\mathbf{k}\cdot\mathbf{R}_{0j}} \left(\frac{1}{R_{0j}^3} - 3\frac{(\mathbf{n}_u \cdot \mathbf{R}_{0j})^2}{R_{0j}^5} \right), \tag{A15}$$

and

$$W_{uv} \to W_{uv}^{(\mathbf{k})} = e^2 \sum_{\mathbf{k}} u_{-\mathbf{k}} v_\mathbf{k} \mathcal{W}_{uv}(\mathbf{k}),$$
$$\mathcal{W}_{uv}(\mathbf{k}) = \sum_j e^{i\mathbf{k}\cdot\mathbf{R}_{0j}} \left(\frac{(\mathbf{n}_u \cdot \mathbf{n}_v)}{R_{0j}^3} - 3\frac{(\mathbf{n}_u \cdot \mathbf{R}_{0j})(\mathbf{n}_v \cdot \mathbf{R}_{0j})}{R_{0j}^5} \right). \tag{A16}$$

Next we perform a unitary rotation of the coordinates $u_\mathbf{k}$, $v_\mathbf{k}$, and $w_\mathbf{k}$, in order to diagonalize the matrix

$$\frac{e^2}{2} \begin{pmatrix} \mathcal{V}_u(\mathbf{k}) & \mathcal{W}_{uv}(\mathbf{k}) & \mathcal{W}_{uw}(\mathbf{k}) \\ \mathcal{W}_{vu}(\mathbf{k}) & \mathcal{V}_v(\mathbf{k}) & \mathcal{W}_{vw}(\mathbf{k}) \\ \mathcal{W}_{wu}(\mathbf{k}) & \mathcal{W}_{wv}(\mathbf{k}) & \mathcal{V}_w(\mathbf{k}) \end{pmatrix}, \tag{A17}$$

which we do numerically. After that the Bogoliubov transformation for each polarization is carried out similar to the way it is done in the main text.

[1] E. Wigner, Phys. Rev. **46**, 1002 (1934).
[2] B. Tanatar and D. M. Ceperley, Phys. Rev. B **39**, 5005 (1989).
[3] N. D. Drummond and R. J. Needs, Phys. Rev. Lett. **102**, 126402 (2009).
[4] C. C. Grimes and G. Adams, Phys. Rev. Lett. **42**, 795 (1979).

[5] E. Y. Andrei, G. Deville, D. C. Glattli, F. I. B. Williams, E. Paris, and B. Etienne, Phys. Rev. Lett. **60**, 2765 (1988); V. J. Goldman, M. Santos, M. Shayegan, and J. E. Cunningham, *ibid.* **65**, 2189 (1990); F. I. B. Williams, P. A. Wright, R. G. Clark, E. Y. Andrei, G. Deville, D. C. Glattli, O. Probst, B. Etienne, C. Dorin, C. T. Foxon, and J. J. Harris, *ibid.* **66**, 3285 (1991); M. A. Paalanen, R. L. Willett, R. R. Ruel, P. B. Littlewood, K. W. West, and L. N. Pfeiffer, Phys. Rev. B **45**, 13784 (1992).

[6] J. Yoon, C. C. Li, D. Shahar, D. C. Tsui, and M. Shayegan, Phys. Rev. Lett. **82**, 1744 (1999).

[7] R. Winkler, *Spin-Orbit Coupling Effects in Two-Dimensional Electron and Hole Systems* (Springer-Verlag, Berlin, 2003).

[8] E. I. Rashba, Fiz. Tverd. Tela (Leningrad) **2**, 1224 (1960) [Sov. Phys. Solid State **2**, 1109 (1960)].

[9] E. Berg, M. S. Rudner, and S. A. Kivelson, Phys. Rev. B **85**, 035116 (2012).

[10] L. Bonsall and A. A. Maradudin, Phys. Rev. B **15**, 1959 (1977).

[11] Technically, this approximation amounts to discarding the cross terms $(\mathbf{r}_i \cdot \mathbf{r}_j)$ and $(\mathbf{r}_i \cdot \mathbf{R}_{ij})(\mathbf{r}_j \cdot \mathbf{R}_{ij})$ in the expansion of Eq. (1).

[12] V. V. Flambaum, I. V. Ponomarev, and O. P. Sushkov, Phys. Rev. B **59**, 4163 (1999).

[13] Or alternatively $a/a_{\mathrm{B}} = r_s(\sqrt{2\pi/\sqrt{3}})$.

[14] S. Gangadharaiah, J. Sun, and O. A. Starykh, Phys. Rev. Lett. **100**, 156402 (2008).

[15] D. Grundler, Phys. Rev. Lett. **84**, 6074 (2000).